ENVIRONMENTAL RESEARCH
LETTERS

ACCEPTED MANUSCRIPT • OPEN ACCESS

Atlantic Multidecadal Variability modulates the climate impacts of El Niño-Southern Oscillation in Australia

To cite this article before publication: Paloma Trascasa-Castro *et al* 2023 *Environ. Res. Lett.* in press https://doi.org/10.1088/1748-9326/ace920

Atlantic Multidecadal Variability modulates the climate impacts of El Niño-Southern Oscillation in Australia.

Paloma Trascasa-Castro[1], Amanda C. Maycock[1], Yohan Ruprich-Robert[2], Marco Turco[3] and Paul W. Staten[4]

[1] Institute for Climate and Atmospheric Science, School of Earth and Environment, University of Leeds, Leeds, UK
[2] Earth Sciences Department, Barcelona Supercomputing Center, Barcelona, Spain
[3] Regional Atmospheric Modelling (MAR) Group, Department of Physics, Regional Campus of International Excellence Campus Mare Nostrum (CEIR), University of Murcia, Murcia, Spain
[4] Department of Earth and Atmospheric Sciences, Indiana University

Corresponding author: Paloma Trascasa-Castro, ee17pt@leeds.ac.uk

Keywords

Atlantic Multidecadal Variability, ENSO, teleconnections, climate impacts, Australia

Abstract

Atlantic Multidecadal Variability (AMV) modulates El Niño-Southern Oscillation (ENSO) dynamics. Here, we explore the effect of warm (AMV+) and cold (AMV-) AMV conditions on the austral summer teleconnection of ENSO to Australia using idealized simulations performed with the NCAR-CESM1 model. AMV+ strengthens the mean and extreme precipitation and temperature responses to El Niño in south-western Australia and weakens the mean precipitation and temperature impacts in north-eastern Australia. The modulation of La Niña impacts by AMV is asymmetric to El Niño, with a weakening of the mean and extreme precipitation and temperature responses in eastern Australia. Decomposing the total difference in ENSO response between AMV phases, we find that the signals are mainly explained by the direct AMV modulation of ENSO and its teleconnections rather than by changes in background climate induced by AMV. The exception is ENSO-driven fire impacts, where there is a significant increase in burned area in south-eastern Australia only when El Niño and AMV+ co-occur. However, modulation of ENSO between AMV+ and AMV- does offset ~37% of the decrease in burned area extent during La Niña summers. The altered surface climate response to ENSO in Australia by AMV is attributed to variations in large-scale atmospheric circulation. Under AMV+, there is increased subsidence over western Australia during El Niño associated with a westward shift of the local Walker circulation. A weakening of the upwelling branch of the local Hadley circulation over north-eastern Australia is responsible for the weakening of La Niña impacts in AMV+, accompanied by a strengthening of subsidence in south central Australia due to a weakening of the local Hadley circulation, amplifying La Niña impacts over this region. The results suggest the potential for AMV to drive multidecadal variability in ENSO impacts over Australia.

1. Introduction

El Niño-Southern Oscillation (ENSO) is the dominant mode of interannual climate variability in the tropics. ENSO impacts remote ecosystems and populations through anomalous atmospheric circulation originating from changes in deep convection in the equatorial Pacific. Anomalous upper-level divergence in the tropics during ENSO alters the Hadley (Trenberth et al. 1998) and Walker circulations, with the upward branch shifting to the central Pacific during El Niño and intensifying over the Maritime continent during La Niña (Walker and Bliss, 1932).

Climate in Australia is strongly influenced by ENSO, especially the northern and eastern regions (Chung and Power, 2017). During El Niño, there is a precipitation deficit in austral spring and summer across Australia. Reduced cloud cover over south-east Australia increases downward shortwave radiation leading to an increase in surface temperature (Arblaster and Alexander, 2012). Higher daily temperatures combined with decreased precipitation under El Niño increases the likelihood of droughts and heatwaves (King et al., 2013). In contrast, during La Niña there is above normal precipitation in northern Australia in austral spring and summer due to the early onset of the monsoon (Drosdowsky et al. 2014). The increase in cloud cover during La Niña leads to cooler temperatures and a weakening of extreme heat episodes during austral summer (Perkins et al. 2015). Australia is one of the most susceptible regions to wildfires in the world (Archibald et al. 2013). While human activity is a dominant source of wildfires in Australia (Marcos et al. 2015), ENSO is an important driver of interannual variability (Abram et al. 2021), which may be superposed onto long-term climate trends (e.g., Dowdy et al. 2019) and multidecadal variability (Canadell et al. 2021).

Recent studies show that decadal climate variability can modulate ENSO behaviour (Ham and Kug, 2015; Levine et al. 2017; Trascasa-Castro et al. 2021). For example, the Interdecadal Pacific Oscillation (IPO) alters the mean background state of the tropical Pacific and modulates ENSO-related impacts over Australia, including changes to seasonal mean impacts (Power et al. 1999), the frequency of extreme precipitation and its potential to lead to flooding events (King et al 2013) and drought risk (Kiem and Franks, 2004). Multidecadal variations in ENSO characteristics may manifest in wildfire frequency and intensity, but the importance of this mechanism is not well quantified due to limited observational records (Liu et al. 2023).

Multidecadal variability in North Atlantic sea surface temperatures (SSTs) can also modulate tropical climate by altering large-scale overturning circulation (Meehl et al., 2020; Liu et al, 2021). Model studies show that the warm phase of Atlantic Multidecadal Variability (AMV+) can drive tropical Pacific cooling (Ruprich-Robert et al. 2017, 2021), although this signal might be overestimated in model simulations with prescribed SSTs in the tropical North Atlantic (O'Reilly et al. 2023). Trascasa-Castro et al. (2021) examined idealised experiments with imposed AMV anomalies and found

that AMV+ damped the amplitude of ENSO by around 10% compared to AMV-. This raises the prospect that the remote impacts of ENSO could be modified by AMV. Past studies found a link between AMV+ and increased precipitation in north-western Australia (Lin and Li 2012). However, there remain uncertainties in the modulation by AMV of ENSO impacts on Australian climate due to the relatively short observational record and the challenge of isolating causal factors in coupled simulations.

This study aims to understand the AMV modulation of ENSO-driven climate impacts in Australia using idealised coupled climate model simulations with imposed AMV conditions. Our results investigate changes in mean surface climate, extreme precipitation and temperature responses to ENSO, and burned area over south-eastern Australia. We further explore the physical mechanisms leading to AMV modulation of ENSO impacts over Australia by decomposing atmospheric circulation changes into contributions from local Hadley and Walker circulations. The paper is laid out as follows: Section 2 describes the simulations and analysis methods. Section 3 presents the results and Section 4 contains the discussion and conclusions of the study.

2. Data and methods

2.1 Climate model simulations

The relatively short observational record hinders the possibility of robustly attributing changes to ENSO variability and teleconnections to AMV, since reliable records cover just one full positive and negative AMV cycle . To overcome this issue, we use idealized experiments performed with the NCAR-CESM1 coupled climate model (Kay et al., 2015), in which time invariant anomalies corresponding to observed warm (AMV+) and cold (AMV-) AMV conditions (Fig. S1) are imposed in the North Atlantic. The model is constrained towards the target AMV SST pattern through Newtonian relaxation of the turbulent surface fluxes, with the ocean and atmosphere being freely coupled outside of the constrained North Atlantic region (from 0 ° to 73° N, with a 8° buffer zones over the northern and southern boundaries. The full restoring is performed between 8° and 65° N. Each simulation lasts for 10 years and a 30 member initial condition ensemble is used, giving a total of 300 years per AMV phase (270 full boreal winter seasons). Further details about the ensemble initialisation are described in Castruccio et al. (2019). The experiments were introduced in Ruprich-Robert et al. (2017) and have been used in several studies (Ruprich-Robert et al. 2018, Castruccio et al., 2019, Meehl et al. 2021, Ruprich-Robert et al. 2021, Trascasa-Castro et al. 2021). The experimental design largely follows the Decadal Climate Prediction Project (DCPP; Boer et al. 2016) Component C experiments within the Coupled Model Intercomparison Project Phase 6 (CMIP6; Eyring et al. 2016).

Zhang et al. (2017) evaluated the performance NCAR-CESM1 in simulating ENSO. The model overestimates SST anomalies associated with La Niña but simulates ENSO skewness relatively well. NCAR-CESM1 captures the sign of ENSO teleconnection to Australia in agreement with observations, although it overestimates the amplitude of precipitation and temperature anomalies particularly in western Australia (Fig. S2).

2.2 Composite analysis

We define the reference climatological state, μ, as the ensemble mean across both AMV+ and AMV- experiments. We define El Niño (La Niña) events in AMV+ or AMV- as austral summers (December-February) where the Niño3.4 index is at least 0.5 K warmer (colder) than in μ. Note this incorporates differences in mean state between AMV+ (μ^+) and AMV- (μ^-) into the identification of ENSO events. The μ^+ minus μ^- climatological DJF Niño3.4 anomaly is -0.23 K. This is larger than the direct modulation of ENSO amplitude between AMV+ and AMV-, which shows an average Nino3.4 anomaly of -0.17 K for El Niño and +0.09 K for La Niña (Trascasa-Castro et al., 2021). The μ^+ minus μ^- difference means that El Niño (La Niña) events will be relatively less (more) frequent, in AMV+ than in AMV-. We adopt this definition because it more closely reflects how observations would be interpreted where interannual variability is superposed on multidecadal variability.

For a given variable, X, we define the mean ENSO impact as the average over all ENSO events in AMV phase η *(either "+" or "-")* minus the reference state μ, such that:

$$\overline{X^\eta} = \sum_{i=1}^{N} X_i^\eta - \mu \quad (1)$$

where X_i^η is the ith El Niño or La Niña event. For each ENSO phase, we estimate the average climate impact independent of AMV, $\bar{X}$, as:

$$\bar{X} = \frac{\overline{X^+}+\overline{X^-}}{2} \quad (2)$$

We define the overall difference in ENSO climate response between AMV+ and AMV-, called hereafter "total modulation of ENSO impacts by AMV" $\Delta\bar{X}$, as:

$$\Delta\bar{X} = \overline{X^+} - \overline{X^-} \quad (3)$$

Conceptually, $\Delta\bar{X}$ can be understood as the sum of the change in mean state driven by AMV ($\Delta\mu$) and the "direct impacts of ENSO modulated by AMV" ($\Delta\overline{X_{ENSO}}$):

$$\Delta\bar{X} = \Delta\mu + \Delta\overline{X_{ENSO}} \quad (4)$$

where

$$\Delta\mu = \mu^{+} - \mu^{-} \quad (5)$$

and

$$\Delta\overline{X_{ENSO}} = (\overline{X^{+}} - \mu^{+}) - (\overline{X^{-}} - \mu^{-}) \quad (6)$$

We note that $\Delta\overline{X_{ENSO}}$ encompasses the modulation of ENSO impacts due to both changes in ENSO teleconnections pathways (because of altered background circulation) and changes in ENSO characteristics (amplitude and/or spatial pattern).

We stress that our decomposition between mean state background changes and modulation of ENSO impacts is not exact (see Supplementary Information). In particular, we implicitly assume that there are no differences in the mean state AMV impact across ENSO phases and attribute those changes to direct ENSO impacts modulated by AMV.

We test for statistical significance by performing a nonparametric bootstrap test subsampling 70% of the 270 austral summer seasons with replacement on each iteration repeated 10^4 times. Differences are estimated to be significant at the 95% confidence level where the ensemble mean anomaly lies outside of 2.5-97.5th percentile range of the bootstrap samples.

2.3 Extreme climate response to ENSO

We analyse the following climate extreme indices (Donat et al. 2013):

- Warm days (TX90p): Number of days per summer season when daily maximum temperature exceeds the local 90th percentile;
- Warm nights (TN90p): Number of days per summer when daily minimum temperature exceeds the local 90th percentile;
- Wet days (R90p): Number of days when precipitation exceeds the local 90th percentile;
- Maximum number of consecutive dry days (CDD) per summer with daily precipitation less than 1 mm.

2.4 Empirical fire model

Burned area (BA) is a widely used metric of wildfire activity that integrates the total number of wildfires occurring over a season and their intensity (Andela et al. 2017). In Australia, the absence of a centralised national database has resulted in the aggregation of data from various fire management agencies in each state and territory (see Data Availability) to construct a comprehensive overview of the countrie's burned areas (Canadell et al. 2021). The data provided by these agencies are represented as polygons in vector files, obtained through diverse sources such as terrestrial mapping, aerial photography, GPS boundary plotting from ground assessments, and remote

sensing. Extensive validation of this data has been conducted, and it has been previously utilized as a reference in numerous studies (e.g., Russell-Smith et al., 2007; Bradstock et al., 2010; Murphy et al., 2013; Canadell et al., 2021). The datasets encompass various types of fires, including both prescribed fires and wildfires. Wildfires are commonly referred to as bushfires in the metadata of these data sources. The term "bushfire" is frequently used to describe vegetation fires in general. Within databases or public warning systems, "bushfires" are categorised as "unplanned fires" or "wildfires," contrasting with "planned fires," "hazard reduction burns," or "prescribed fire". We focus on changes in BA in the eastern Australian temperate forest region (Dinerstein et al. 2017), which is highly populated, vulnerable to wildfires and has a 50-year fire data record. We aggregate all the wildfires whose centre of gravity falls in the study domain and which start in the fire season from September-February (Canadell et al., 2021). A fire year is defined by the year in which the fire season ends.

The Standardized Precipitation Evapotranspiration Index (SPEI) estimates the relationship between preconditioning meteorological conditions and the BA during the fire season, following Turco et al. (2018). SPEI accounts for total accumulated precipitation and potential evapotranspiration (PET). The Hargreaves method is used to estimate PET, including temperature and precipitation in its formulation (plus the latitudinal correction factor). We calculate the observed SPEI over 1971–2020 using monthly mean maximum near-surface temperature and precipitation from the Climate Research Unit dataset (CRU_TS4.06, Harris et al., 2020). Climate variables are spatially averaged over the southeast Australia domain for the analysis (Fig. 5a).

As in Turco et al. (2018), we express the SPEI-BA model as:

$$log[BA(sc,m)] = \beta 1 + \beta 2 \cdot SPEI(sc,m) + \varepsilon(sc) \text{ (eq. 7)},$$

where *sc* is the timescale (varying from 1 to 12 months) used to compute the SPEI, *m* is the month for which the SPEI is computed (varying from September to February) and ε refers to noise caused by sources of BA variability other than the SPEI.

To find the highest fraction of variance explained, we calculate all the possible regression models by varying *sc* and *m*. The selected model explains 56% of the BA variability based on the $SPEI_{5,Jan,}$ i.e. the climate data aggregated from September to January. We apply the empirical observed relationship from Eq. 7 to the NCAR-CESM1 AMV+ and AMV- output to determine effective changes in BA by AMV.

2.5 Atmospheric circulation decomposition into local Walker and Hadley components

To match regions of anomalous veritcal motion to changes in the large-scale circulation we perform a Helmholtz decomposition of the flow after Schwendike et al. (2014). Recognising that the tropical circulation is dominated by large-scale zonal (Walker) and meridional (Hadley) overturning circulations, which may have distinct mechanisms, this approach enables us to quantify the relative importance of Walker

and Hadley circulations for the local circulation response, and associated climatic changes, over Australia.

We use spherical harmonics to isolate the divergent wind field from the full wind field. Then we use the kinematic method to calculate the component of ascent due to meridional (or zonal) overturning from the divergence of the meridional (or zonal) component of the divergent wind. This decomposition gives us the local Hadley and Walker components of large-scale ascent (Schwendike et al. 2014).

3. Results

3.1 AMV modulation of ENSO mean climate impacts over Australia

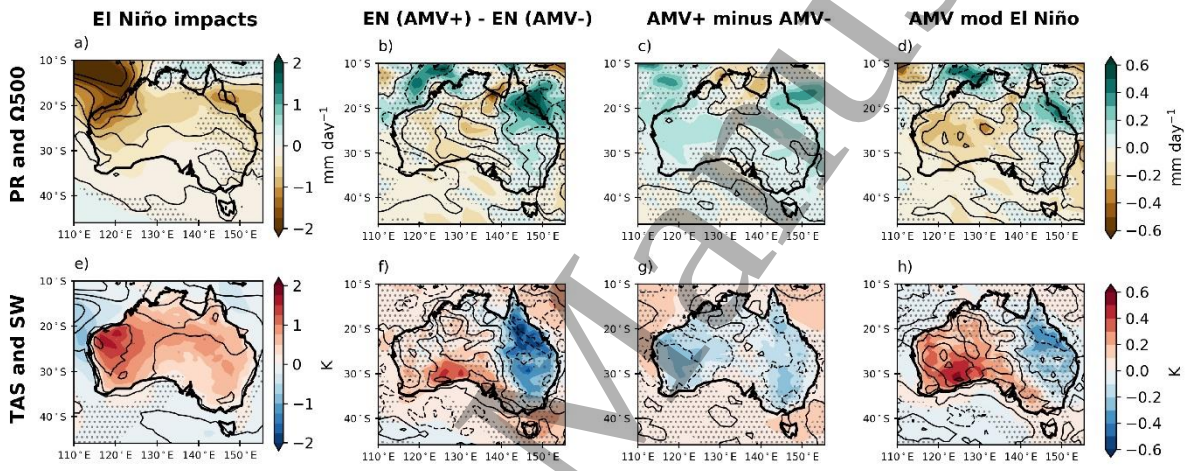

Figure 1. El Niño-related impacts over Australia in DJF. Top: precipitation (mm day^{-1}) in shading and vertical velocity at 500 hPa (Pa s^{-1}) with contours at ±0.02 Pa s^{-1} (a) and ±0.01 Pa s^{-1} (b, c and d). Bottom: near-surface temperature (K) in shading and net surface shortwave radiation with contours ±30 W m^{-2} (e) and ±10 W m^{-2} (f, g and h). Columns show: (a,e) Mean El Niño impacts (eq. 2); (b,f) the total El Niño modulation by AMV (eq. 3); (c,g) the mean background change due to AMV (eq. 5); and (d,h) the direct AMV modulation of El Niño impacts (eq. 6). Dotted areas denote absence of statistical significance in the precipitation (top) and near-surface temperature (bottom) at the 95% confidence level.

El Niño leads to a precipitation deficit and increased subsidence over Australia (Fig. 1a). Higher mean surface temperatures occur alongside increased net surface shortwave (SW) radiation (Fig. 1e). The strong spatial resemblance between anomalous surface SW radiation and mid-level vertical velocity (Fig. 1e) suggests anomalies in mean surface temperature are related to changes in large-scale atmospheric dynamics rather than local processes. During La Niña, the anomalies are of a similar amplitude but opposite sign (Figs. 2a, e).

The total El Niño modulation by AMV (Eq. 3) (Fig. 1b and f) shows a weaker precipitation decrease above 0.6 mm day^{-1} over north-east Australia, along with a damping of the local subsidence seen in the mean El Niño response (compare contours between Fig. 1b and Fig. 1a). Alongside the weakening of El Niño-related

precipitation, there is a weakening of mean near-surface warming of -0.6 K associated with reduced incoming SW radiation (Fig. 1f). In contrast, there is a slight strengthening of the El Niño impacts over south-central Australia under AMV+, with an increase in temperature of up to 0.4 K and a small but significant increase in precipitation deficit.

The total modulation of La Niña by AMV (Fig. 2b,e) displays a similar amplitude but opposite sign to that found for El Niño (Fig. 1b,e). However, the spatial locations of the anomalies differ, highlighting the asymmetry in the AMV modulation of ENSO impacts in Australia. In particular, the total modulation pattern in near-surface temperature during La Niña is shifted by 5° to the east compared to El Niño.

As explained in Section 2.2, the total modulation of ENSO impacts by AMV can be understood as the sum of the change in background climate between AMV phases (Eq. 5) and the direct modulation of ENSO characteristics and/or its teleconnections by AMV (Eq. 6). The mean state difference between AMV+ and AMV- is characterised by wetting and cooling over western and eastern Australia of up to 0.2 mm day^{-1} and 0.2 K, respectively (Fig. 1c,g). Therefore, the mean climate response to AMV+ tends to offset the total El Niño impacts over Australia compared to AMV-. This is consistent with the fact that, on average, in these experiments AMV+ drives tropical Pacific cooling, pushing the climate state towards a La-Niña like background state (Ruprich-Robert et al. 2017, Trascasa-Castro et al. 2021). Once the mean state changes are subtracted from the total modulation, we observe an east-west dipole pattern characterising the direct modulation of ENSO impacts by AMV (Figs. 1d,h; 2d,h), with a strengthening of the surface response to ENSO over southwestern Australia and a weakening of ENSO impacts over eastern Australia in austral summer.

Overall, the differences in the total modulation of ENSO impacts over Australia by AMV are primarily driven by the direct modulation of ENSO impacts by AMV and not mean state changes.

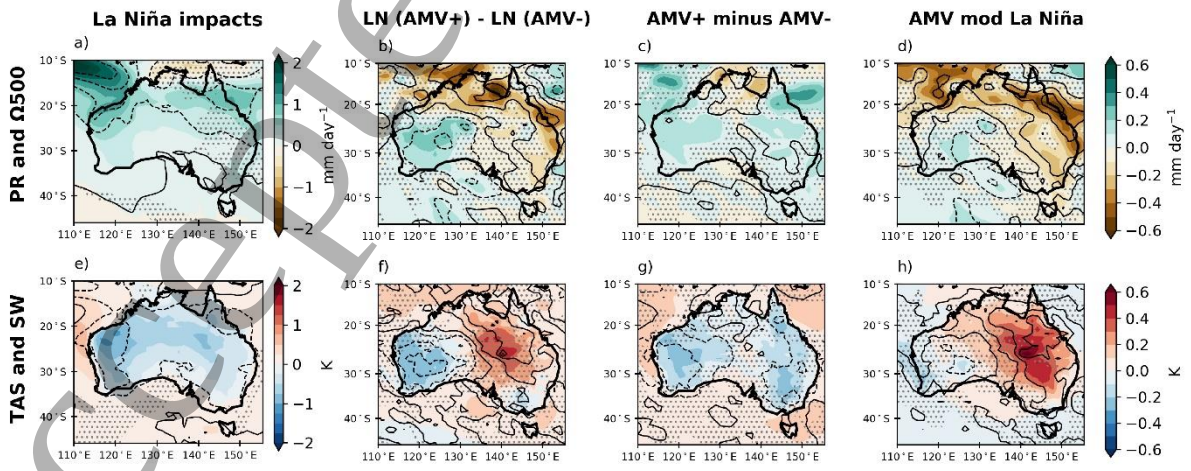

Figure 2. As in Figure 1 but for La Niña. Panels c and g are identical to Fig. 1 by construction.

3.2 AMV modulation of ENSO-driven climate extremes over Australia

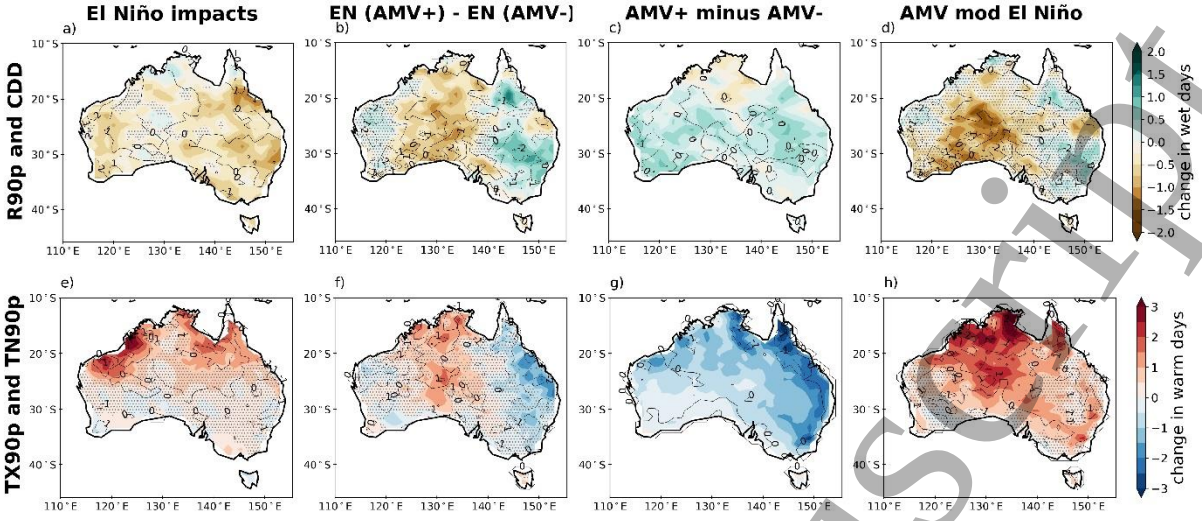

Figure 3. El Niño-related extremes over Australia in DJF. Top: change in no. wet days (R90p; shading) and consecutive dry days per summer (CDD; contours. Contour interval is 1 day). Bottom: change in no. warm days (TX90p; shading) and warm nights (TN90p; contours. Contour interval is 1 night). Columns show: (a,e) Mean El Niño impact (eq. 2); (b,f) the total El Niño modulation by AMV (eq. 3); (c,g) the mean change due to AMV (eq. 5); and (d,h) the direct AMV modulation of El Niño impacts (eq, 6). Stippled areas show non-significant anomalies in R90p (top) and TX90p (bottom) at the 95% confidence level.

After showing that AMV modulates the summer mean ENSO-climate signals in Australia in NCAR-CESM1, primarily by modulating ENSO impacts, we now explore changes in daily precipitation and temperature extremes.

During El Niño, eastern Australia experiences a decrease in the number of summer wet days (Fig. 3a). There are up to 3 more warm days per summer in the north and north-west of Australia (Fig. 3e), and the period with CDD extends by one day. La Niña summers are characterised by anomalies that are equivalent in amplitude but opposite in sign to El Niño (Figs. 4 a and e).

The total modulation of El Niño-driven extremes by AMV shows a signal of 1 extra wet day per summer over eastern Australia associated with a decrease in CDD (Fig. 3b), and a decrease in R90p over the central part of Australia between 125°E-135°E, where there is also an increase of 1 extra warm day and night per summer (Fig. 3f). The total modulation of La Niña temperature extremes by AMV is stronger, with 2 more warm days and nights in eastern Australia (Fig. 4f). The magnitude of the total modulation of ENSO-driven changes in extremes by AMV is comparable to the mean ENSO signal in NCAR-CESM1, representing a substantial modification that may manifest on multi-decadal timescales.

The changes in precipitation extremes attributable to the mean climate response to AMV extend rather homogeneously across Australia (Fig. 3c); however, changes to temperature extremes are largest over northern and eastern regions (Fig. 3g). AMV modulation of the direct ENSO impacts on extreme precipitation and temperature

(Figs. 3d, h and 4d, h) resemble the apparent differences in ENSO impacts shown in Figs. 3b, f and 4b, f, but with stronger relative amplitudes. In AMV+, the El Niño signal intensifies over central and southern Australia, evidenced by a decrease of 2 in R90p, and an increase in CDD. There is also an overall increase of up to 3 warm days and 2 warm nights per summer, peaking over the North of Australia. The AMV modulation of La Niña consists of a weakening of the mean La Niña response (Figs. 4a,e), with a significant decrease in R90p over eastern and Western Australia (Fig. 4d), and a larger increase of up to 3 warm and nights over eastern Australia (Fig. 4. h).

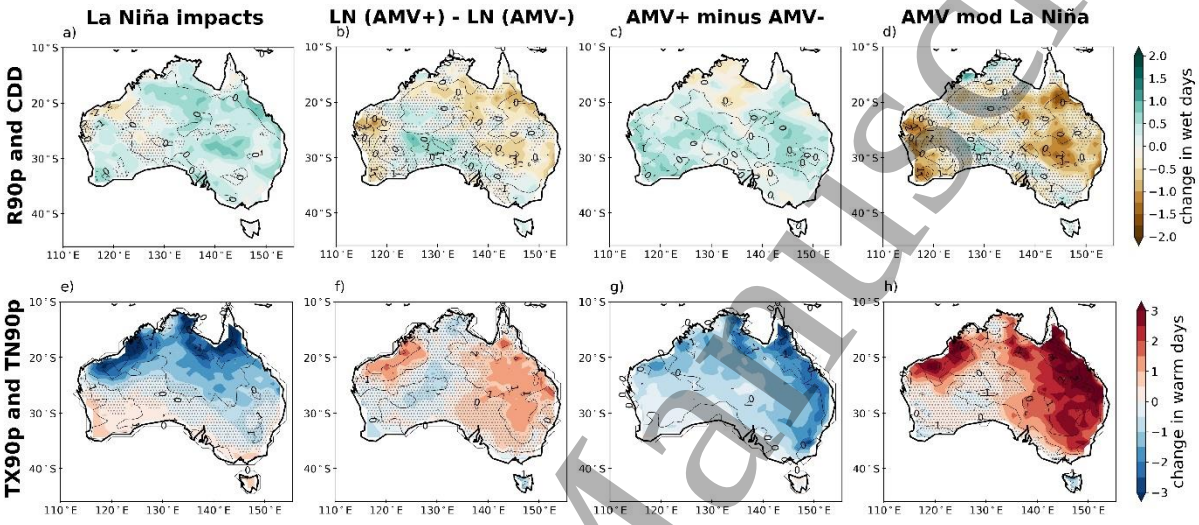

Figure 4. As in Fig. 3 but for La Niña. Panels c and g are identical to Fig. 3 by construction.

In comparison to the direct modulation of ENSO impacts by AMV (Figs. 1 and 2, right column), changes in extreme precipitation and temperature do not show a clear dipole with intensification over the west and weakening over the east (Fig. 3 and 4, right column). This reveals that the AMV modulation of ENSO extremes is not only asymmetric as ENSO mean impacts, but it is also nonlinear. Comparing Figs. 1h and 3h one can see a different pattern of the AMV modulation of ENSO TAS in DJF (Fig. 1h) and TX90P (Fig. 3h). In Fig. 1h the dipole consisting of an amplification of the surface temperature response to El Niño in DJF is very noticeable, with an amplification of warm conditions over the south-west and a decrease in temperature over the north-east. In contrast the AMV modulation of warm days during El Niño consists of an overall amplification of the mean signal, with an increase in warm days that is strongest in the north. The mean El Niño impacts in Figs. 1a,e and 3a,e show that areas where seasonal mean anomalies are strongest do not necessarily coincide with the changes in extreme diagnostics. A similar situation is shown in Figs. 2 and 4 (La Niña). Therefore, further investigation is required to understand the differences in the spatial patterns of the AMV modulation of ENSO mean and extreme impacts.

3.3 AMV modulation of ENSO-driven fire activity over Australia

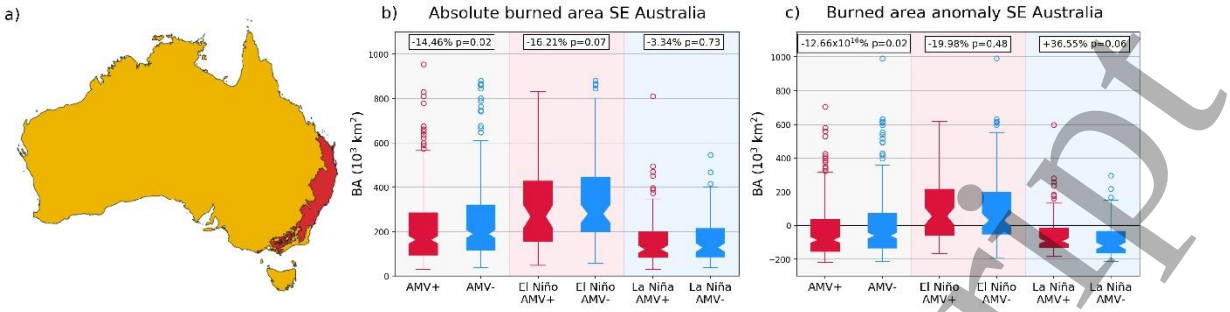

Figure 5. a) Focus area for the wildfire study (shaded in red). (b) Boxplots of absolute burned area (km^2) in SE Australia estimated using NCAR-CESM1 output with the empirical SPEI-BA relationship derived from observations using Eq 7. (c) Anomalies in burned area (km^2) with respect to the mean state of the matched AMV phase. Red (blue) boxplots show values in AMV+ (AMV-). Numbers on top show the % difference between El Niño (or La Niña) in AMV+ and AMV- and their associated p-value estimated with a two-sided Student's t-test.

Given the significant AMV modulation of the ENSO climate impacts over Australia in NCAR-CESM1, we make the further step to explore the implication for forest fires over south-eastern Australia (Fig. 5a) using the statistical model introduced in Section 2.2. The SPEI12 was chosen as an estimator of burned area, meaning that precipitation and temperature 12 months prior to the end of the fire season were considered. We considered other frequencies of SPEI and found no significant changes in the AMV modulation of the ENSO-BA relationship in Australia. Figure 5b shows BA in each AMV phase (red AMV+, blue AMV-) and for El Niño (middle column) and La Niña (right column) events during each AMV phase. BA decreases significantly by 14.5% in AMV+ compared to AMV-. There is also a borderline significant (p-value < 0.07) decrease in BA of 16.2% during El Niño in AMV+ compared to AMV-. During La Niña, there are no statistically significant BA changes between AMV phases. The fact that ENSO and AMV signals are superimposed in Fig. 5b hinders the isolation of the proportion of ENSO-driven BA that is actually modulated by AMV.

To quantify the AMV modulation of direct ENSO impacts, we remove the mean background AMV signal and show the results as anomalies relative to each AMV mean state (Fig. 5c). This shows that the dAMV modulation of the direct El Niño-driven BA is not significant, but there is a significant offset of the decrease in BA during La Niña of around 37% (p-value < 0.06). As shown in Figs. 2d and 2h, the precipitation and temperature anomalies driven by La Niña in the south-east of Australia is damped by AMV+. Drier and warmer conditions induced by AMV+ increase the risk of fire weather during La Niña summers. During El Niño, the significant reduction in south-east Australia BA by AMV is due to the mean background climate effects rather than the modulation of the direct El Niño impacts by AMV.

3.3 AMV modulation of large-scale circulation leading to climate impacts

To understand the origins of the modulation of ENSO climate impacts discussed in Sections 3.1 and 3.2, we next examine the large-scale circulation response. In particular, we explore the physical origin of the modulation of the mid-tropospheric subsidence anomalies over Australia using the decomposition into local Hadley and Walker circulation components described in Section 2.5.

During El Niño, there is a shift in tropical convection from the warm pool towards the central equatorial Pacific resulting in negative 500 hPa pressure velocity anomalies and a weakening of the South Pacific Convergence Zone (SPCZ) (Fig. 6a). This response is mainly associated with changes in the local Hadley circulation (Fig. 6e), with the pressure velocity anomalies associated with the local Walker component (Fig. 6i) being roughly three times weaker. The total modulation by AMV of the local Hadley component response to El Niño (Fig. 6f) shows a weakening of the enhanced upward motion in the central equatorial Pacific, especially between 150-180°E. Between 15ºS-15ºN, this total modulation is explained by a general decrease of the El Niño impacts by the mean state change (Fig. 6h) and by a westward shift/extension of the canonical El Niño impacts by the AMV modulation of the El Niño impacts (Fig. 6h; see also Fig. S3), in agreement with Trascasa-Castro et al. (2021)

Over Australia, the mean El Niño signal in pressure velocity comprises increased subsidence particularly over northern regions (Fig 6a). The total modulation of the vertical velocity response to El Niño by AMV (Fig. 6b) consists of intensified subsidence over central Australia with a similar contribution of the local Hadley and local Walker components. The changes in the Walker circulation can be explained mostly by the mean state AMV impact (Fig. 6k). Under warm AMV conditions (Figs. 6g and 7g), the deep convection associated with the ascending branch of the Hadley cell in the Pacific is shifted North during boreal winter, and the SPCZ loses strength. This is in broad agreement with observational and modelling studies linking AMV to changes in Hadley circulation pattern and strength (Zplotnik et al. 2022, Liu et al., 2020).

Regarding the direct modulation of El Niño impacts, AMV+ enhances subsidence over central-western Australia and weakens ascent over Western Australia (Fig. 6d). This seems to be driven by a westward shift of the mean El Niño signature over Australia, which echoes the westward shift of the vertical velocity in the deep tropics (Fig. S3ac). The dipole structure of the vertical velocity anomalies over Australia is reminiscent of the dipole anomalies already discussed for surface temperature and precipitation (Fig. 1a,e).

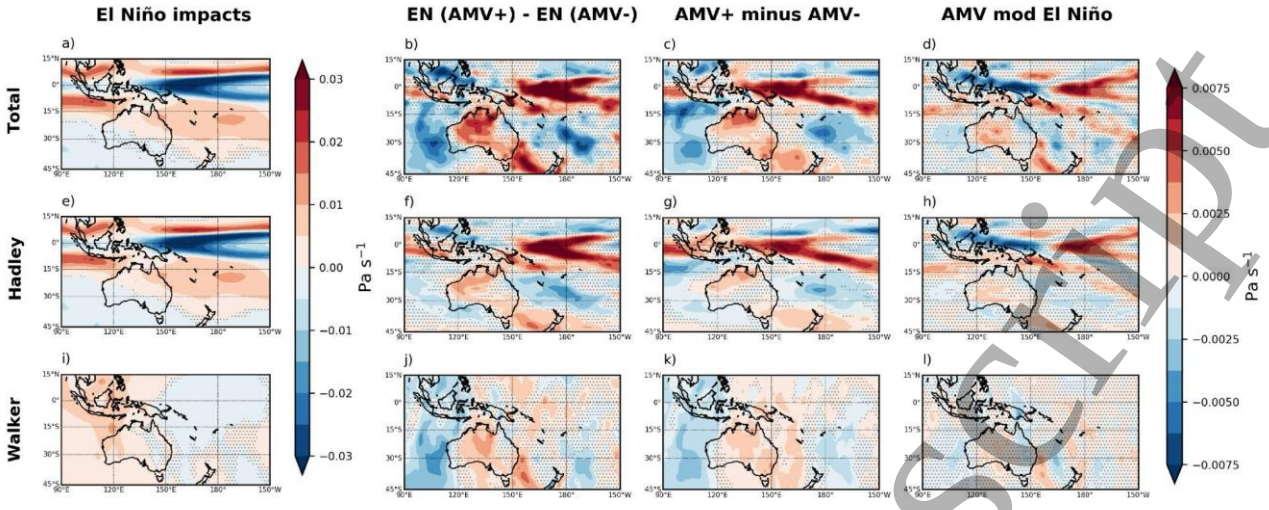

Figure 6. El Niño-related vertical velocity at 500 hPa (Pa s^{-1}) in DJF. Top row: total change, middle row: local Hadley component and bottom row: local Walker component. Columns show: (a,e,i) Mean El Niño impact (eq. 2); (b,f,j) the total El Niño modulation by AMV (eq. 3); (c,g,k) the mean change due to AMV (eq. 5); and (d,h,l) the direct AMV modulation of El Niño impacts (eq, 6). Negative values show ascent and positive values descent. Stippled areas show non-significant anomalies at the 95% confidence level.

The mean La Niña signal is reduced upwelling in the equatorial Pacific (Fig. 7a), predominantly associated with the local Hadley circulation (Fig. 7e) with only a small role for local Walker circulation changes (Fig. 7i). Over eastern Australia, AMV+ weakens the total La Niña anomalies causing enhanced subsidence over the eastern coast (Fig. 7b), driven by both the direct AMV modulation of La Niña impacts (Fig. 7d) and the mean state AMV changes (Fig. 7c). This modulation is mainly caused by a weakening of the local Hadley circulation impacts (Fig. 7h vs Fig. 7e), with a minor contribution of the local Walker component (Fig. 7l). Over the western part of the country, AMV+ enhances the upward motion of air during La Niña summers (Fig. 7bd), driven by a strengthening of the zonal overturning circulation by modulating the direct La Niña impacts (Fig. 7l).

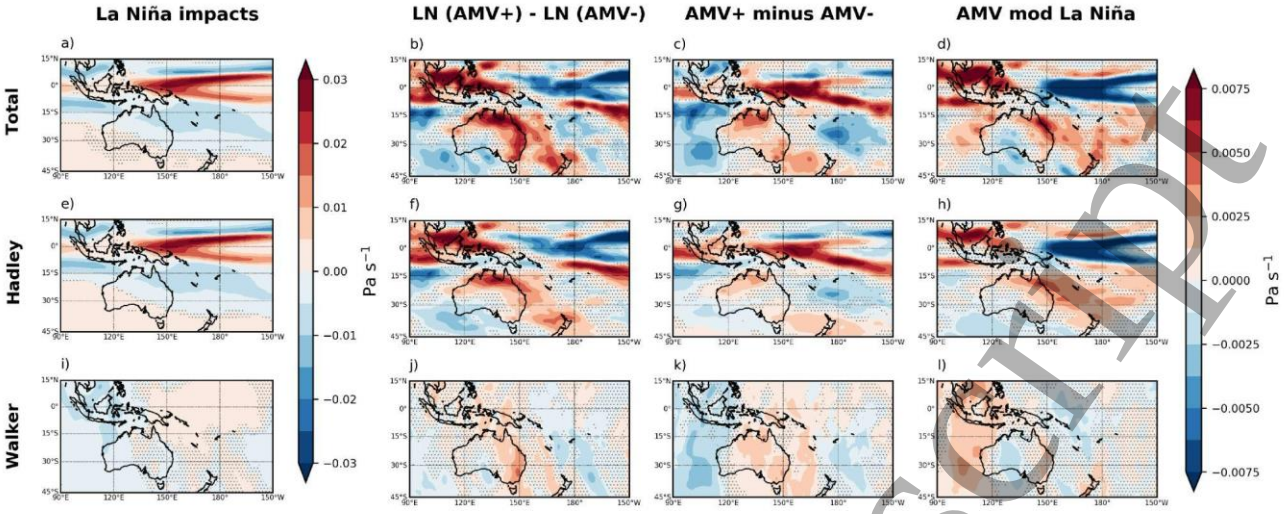

Figure 7. As in Fig. 6 but for La Niña. Panels c, g and k are identical to Fig. 6 by construction.

4. Discussion and conclusions

We analysed idealised model experiments to investigate how ENSO impacts on Australian climate are modulated by AMV. The large ensemble experiments with 270 austral summers of perpetual AMV+/- conditions offer a large sample that allows a cleaner separation of the effects of AMV-ENSO interactions than can be achieved in the limited instrumental record. The total modulation of ENSO impacts by AMV (i.e. what one would observe in the real world) can be decomposed into a background state change due to AMV and a signal from modulation of the direct ENSO impacts by AMV, the latter implicitly includes effects from changes in ENSO characteristics and/or changes in teleconnections.

This is an advance over some earlier studies where these components have not been explicitly separated Maher et al. (2022), allowing contributing mechanisms from mean state changes and direct ENSO modulation to be distinguished. The study builds on the results of Trascasa-Castro et al. (2021) who showed a weakening of ENSO amplitude in the simulations by ~10%. We highlight in our decomposition that the modulation of ENSO by AMV can include effects from changes in ENSO patterns and the altered atmospheric response to this pattern.

An east-west dipole pattern, with warm AMV conditions strengthening (weakening) ENSO impacts over western (eastern) Australia, is found for changes in mean summer precipitation and temperature. Under El Niño (La Niña), the mean background state change due to AMV enhances (diminishes) the direct modulation of impacts by AMV in eastern Australia, with the opposite found in western Australia.

The reduction in wet days across most of Australia under El Niño is negated by the AMV modulation in eastern regions but is enhanced in central and southern regions. Though the background state change by AMV leads to an increase in wet days across

Australia, the direct modulation of El Niño impacts by AMV leads to a relatively stronger decrease in southern and central regions. In contrast, La Niña increases the frequency of wet days across most of Australia, with the total modulation by AMV muting this signal in eastern Australia making extreme wet days less likely in this region during AMV+. While the canonical El Niño response shows increases in warm days and nights confined to northern Australia, the direct modulation of ENSO impacts by AMV shows a reduction of warm days and nights in eastern Australia and increase in central Australia, and vice versa for La Niña. This east-west dipole resembles the pattern seen for seasonal mean precipitation and temperature modulation by AMV.

The east-west dipole across Australia seen in the total modulation of ENSO impacts by AMV on several climate indicators can be explained by changes in the equatorial Pacific atmospheric circulation. AMV drives background changes that project on a La Niña-like state (Ruprich-Robert et al. 2017, Trascasa-Castro et al. 2021), which are associated with changes in the Walker and Hadley circulations, mostly weakening the total El Niño teleconnections but strengthening the La Niña ones (Figs. 6cgk, 7cgk and S3). The AMV also modulates the ENSO characteristics, with weaker ENSO events and westward shifted El Niño events (i.e. more Central Pacific like) during AMV+ (Figs. 6dhl, 7dhl and S3), in agreement with the previous study of Trascasa-Castro et al. (2021). The east-west dipole across Australia seen in the total modulation of many ENSO impacts appears also explained by the combination of a La Niña-like background change and by a westward shift of ENSO teleconnections. We note that the AMV modulation of ENSO described here would incorporate the modulation of ENSO characteristics, e.g. a change in the frequency of central and eastern Pacific events, as well as modulation of ENSO teleconnections by the altered background state. Future work could be done to separate these two aspects.

The results show no significant modulation of ENSO anomalies in burned area in south-east Australia by AMV, but during AMV- mean burned area is significantly higher than during AMV+. This finding contrasts with Liu et al. (2023), who explore the AMV modulation of the relationship between the autumn Niño3.4 index and the Fire Weather Index (FWI). They find a positive correlation between ENSO and Australian FWI in observations, with the relationship being stronger in AMV+ than in AMV-. Opposite to what our results show, they suggest that AMV+ reinforces the El Niño-driven hot and dry conditions over Australia given the warm and dry anomalies driven by AMV in austral spring. Therefore, uncertainty remains in the sign of the AMV modulation of ENSO-driven burned area variability in Australia and further work is needed to understand the sources of uncertainty and constrain the relationship.

The mechanisms proposed here could ultimately contribute to multidecadal variability in ENSO impacts, meaning that Australian climate may undergo periods of apparently more severe or muted climate variability on interannual timescales. Should such variability arise in observations, it would be superposed onto background climate trends driven by external forcings like greenhouse gases. Eastern Australia has

already experienced a rapid drying trend due to anthropogenic emissions of greenhouse gases (Abram et al. 2021). Hence, multidecadal variability may affect overall resilience and adaptation to climate extremes in a warming world, and hence internal variability should be considered within storylines for Australian climate change and stress testing against weather and climate extremes.

5. Acknowledgments and Data Availability Statement

The DCPP NCAR-CESM1 data are available through the CMIP6 archive on the Earth System Grid Federation.

State	**Agency**	**URL**
New South Wales	Department of Planning, Industry and Environment	https://datasets.seed.nsw.gov.au/dataset/fire-history-wildfires-and-prescribed-burns-1e8b6
Queensland	Queensland Parks and Wildlife Service	https://qldspatial.information.qld.gov.au/catalogue/custom/
Victoria	Department of Environment, Land, Water & Planning	https://discover.data.vic.gov.au/dataset/fire-history-records-of-fires-primarily-on-public-land

6. References

Abram, N. J., B. J. Henley, A. S. Gupta, T. J. Lippmann, H. Clarke, A. J. Dowdy, J. J. Sharples, R. H. Nolan, T. Zhang, M. J. Wooster, J. B. Wurtzel, K. J. Meissner, A. J. Pitman, A. M. Ukkola, B. P. Murphy, N. J. Tapper, and M. M. Boer. (2021). Connections of climate change and variability to large and extreme forest fires in southeast Australia. *Communications Earth Environment* 2:1, 2(1):1–17. ISSN 2662-4435. doi: 10.1038/s43247-020-00065-8.

Andela, N., Morton, D. C., Giglio, L., Chen, Y., van der Werf, G. R., Kasibhatla, P. S., ... & Randerson, J. T. (2017). A human-driven decline in global burned area. *Science*, 356(6345), 1356-1362.

Arblaster, J. M., & Alexander, L. V. (2012). The impact of the El Niño-Southern Oscillation on maximum temperature extremes. *Geophysical Research Letters*, *39*(20).

Archibald, S., C. E. Lehmann, J. L. Gomez-Dans, and R. A. Bradstock. Defining pyromes and global syndromes of fire regimes (2013). *Proceedings of the National Academy of Sciences of the United States of America*, 110(16):6442–6447. ISSN 00278424. doi: 10.1073/PNAS. 1211466110/SUPPL FILE/PNAS.201211466SI.PDF.

Boer, G. J., Smith, D. M., Cassou, C., Doblas-Reyes, F., Danabasoglu, G., Kirtman, B., ... & Eade, R. (2016). The decadal climate prediction project (DCPP) contribution to CMIP6. *Geoscientific Model Development*, *9*(10), 3751-3777.

Bradstock, R. A. (2010). A biogeographic model of fire regimes in Australia: current and future implications. Global Ecology and Biogeography, 19(2), 145-158.

Cai, W., Santoso, A., Wang, G., Wu, L., Collins, M., Lengaigne, M., ... & Timmermann, A. (2020). ENSO response to greenhouse forcing. *El Niño Southern Oscillation in a Changing Climate*, 289-307.

Canadell, J. G., Meyer, C. P., Cook, G. D., Dowdy, A., Briggs, P. R., Knauer, J., ... & Haverd, V. (2021). Multi-decadal increase of forest burned area in Australia is linked to climate change. *Nature Communications*, 12(1), 1-11.

Castruccio, F. S., Ruprich-Robert, Y., Yeager, S. G., Danabasoglu, G., Msadek, R., & Delworth, T. L. (2019). Modulation of Arctic sea ice loss by atmospheric teleconnections from Atlantic multidecadal variability. *Journal of Climate*, *32*(5), 1419-1441.

Chung, C. T. and S. B. Power, (2017). The non-linear impact of El Niño, La Niña and the Southern Oscillation on seasonal and regional Australian precipitation. *Journal of Southern Hemisphere Earth Systems Science*, 67(1):25–45. ISSN 22065865. doi: 10.22499/3.6701.003.

Dinerstein, E., Olson, D., Joshi, A., Vynne, C., Burgess, N. D., Wikramanayake, E., ... & Saleem, M. (2017). An ecoregion-based approach to protecting half the terrestrial realm. *BioScience*, 67(6), 534-545.

Donat, M. G., Alexander, L. V., Yang, H., Durre, I., Vose, R., Dunn, R. J., ... & Kitching, S. (2013). Updated analyses of temperature and precipitation extreme indices since the beginning of the twentieth century: The HadEX2 dataset. *Journal of Geophysical Research: Atmospheres*, *118*(5), 2098-2118.

Dowdy, A. J., H. Ye, A. Pepler, M. Thatcher, S. L. Osbrough, J. P. Evans, G. Di Virgilio, and N. McCarthy, (2019). Future changes in extreme weather and pyroconvection risk factors for Australian wildfires. *Scientific Reports* 9:1, 9(1):1–11. ISSN 2045-2322. doi: 10.1038/s41598-019-46362-x.

Drosdowsky, W., & Wheeler, M. C. (2014). Predicting the onset of the north Australian wet season with the POAMA dynamical prediction system. *Weather and forecasting*, *29*(1), 150-161.

Eyring, V., Bony, S., Meehl, G. A., Senior, C. A., Stevens, B., Stouffer, R. J., & Taylor, K. E. (2016). Overview of the Coupled Model Intercomparison Project Phase 6 (CMIP6) experimental design and organization. Geoscientific Model Development, 9(5), 1937-1958.

Ham, Y. G., & Kug, J. S. (2015). Role of north tropical Atlantic SST on the ENSO simulated using CMIP3 and CMIP5 models. *Climate Dynamics*, *45*, 3103-3117.

Harris, S., & Lucas, C. (2019). Understanding the variability of Australian fire weather between 1973 and 2017. *PLoS one*, *14*(9), e0222328.

Harris, I., Osborn, T. J., Jones, P., & Lister, D. (2020). Version 4 of the CRU TS monthly high-resolution gridded multivariate climate dataset. *Scientific Data*, *7*(1), 109.

Kay, J. E., Deser, C., Phillips, A., Mai, A., Hannay, C., Strand, G., et al. (2015). The Community Earth System Model (CESM) large ensemble project: A community resource for studying climate change in the presence of internal climate variability. *Bulletin of the American Meteorological Society*, 96(8), 1333–1349. https://doi.org/10.1175/bams-d-13-00255.1

Kiem, A. S., & Franks, S. W. (2004). Multi-decadal variability of drought risk, eastern Australia. *Hydrological Processes*, *18*(11), 2039-2050.

King, A. D., L. V. Alexander, and M. G. Donat. Asymmetry in the response of eastern Australia extreme rainfall to low-frequency Pacific variability, (2013). *Geophysical Research Letters,* 40(10):2271–2277.

Levine, A. F., McPhaden, M. J., & Frierson, D. M. (2017). The impact of the AMO on multidecadal ENSO variability. *Geophysical Research Letters*, *44*(8), 3877-3886.

Lin, Z., & Li, Y. (2012). Remote influence of the tropical Atlantic on the variability and trend in North West Australia summer rainfall. *Journal of Climate*, *25*(7), 2408-2420.

Liu, Y., Gong, Z., Sun, C., Li, J., & Wang, L. (2020). Multidecadal seesaw in Hadley circulation strength between the two hemispheres caused by the Atlantic multidecadal variability. *Frontiers in Earth Science*, *8*, 580457.

Liu, G., Li, J., & Ying, T. (2023). Atlantic Multi-decadal Oscillation Modulates the Relationship Between El Niño-Southern Oscillation and Fire Weather in Australia. *Atmospheric Chemistry and Physics Discussions*, *2023*, 1-17.

Marcos, R., Turco, M., Bedía, J., Llasat, M. C., & Provenzale, A. (2015). Seasonal predictability of summer fires in a Mediterranean environment. *International journal of wildland fire*, 24(8), 1076-1084.

Maher, N., Kay, J. E., & Capotondi, A. (2022). Modulation of ENSO teleconnections over North America by the Pacific decadal oscillation. *Environmental Research Letters*, *17*(11), 114005.

Meehl, G. A., Hu, A., Castruccio, F., England, M. H., Bates, S. C., Danabasoglu, G., ... & Rosenbloom, N. (2021). Atlantic and Pacific tropics connected by mutually interactive decadal-timescale processes. Nature Geoscience, 14(1), 36-42.

Murphy, B. P., Bradstock, R. A., Boer, M. M., Carter, J., Cary, G. J., Cochrane, M. A., ... & Bowman, D. M. (2013). Fire regimes of a ustralia: A pyrogeographic model system. Journal of Biogeography, 40(6), 1048-1058.

O'Reilly, C. H., Patterson, M., Robson, J., Monerie, P. A., Hodson, D., & Ruprich-Robert, Y. (2023). Challenges with interpreting the impact of Atlantic Multidecadal Variability using SST-restoring experiments. *npj Climate and Atmospheric Science*, *6*(1), 14.

Perkins, S. E., Argüeso, D., & White, C. J. (2015). Relationships between climate variability, soil moisture, and Australian heatwaves. Journal of Geophysical Research: Atmospheres, 120(16), 8144-8164.Power, S., T. Casey, C. Folland, A. Colman, and V. Mehta, (1999). Inter-decadal modulation of the impact of ENSO on Australia. *Climate Dynamics*, 15(5):319–324. ISSN 1432-0894. doi:10.1007/s003820050284.

Ruprich-Robert, Y., R. Msadek, F. Castruccio, S. Yeager, T. Delworth, and G. Danabasoglu, (2017) Assessing the climate impacts of the observed atlantic multidecadal variability using the GFDL CM2.1 and NCAR CESM1 global coupled models. *Journal of Climate,* 30(8):2785–2810. ISSN 08948755. doi: 10.1175/JCLI-D-16-0127.1.

Ruprich-Robert, Y., Delworth, T., Msadek, R., Castruccio, F., Yeager, S., & Danabasoglu, G. (2018). Impacts of the Atlantic multidecadal variability on North American summer climate and heat waves. Journal of Climate, 31(9), 3679-3700.

Ruprich-Robert, Y., Moreno-Chamarro, E., Levine, X., Bellucci, A., Cassou, C., Castruccio, F., ... & Tourigny, E. (2021). Impacts of Atlantic multidecadal variability on the tropical Pacific: a multi-model study. *npj climate and atmospheric science*, *4*(1), 33.

Russell-Smith, J., Yates, C. P., Whitehead, P. J., Smith, R., Craig, R., Allan, G. E., ... & Gill, A. M. (2007). Bushfires 'down under': patterns and implications of contemporary Australian landscape burning. International Journal of Wildland Fire, 16(4), 361-377.

Schwendike, J., Govekar, P., Reeder, M. J., Wardle, R., Berry, G. J., & Jakob, C. (2014). Local partitioning of the overturning circulation in the tropics and the connection to the Hadley and Walker circulations. *Journal of Geophysical Research: Atmospheres*, *119*(3), 1322-1339.

Staten, P. W., Grise, K. M., Davis, S. M., Karnauskas, K., & Davis, N. (2019). Regional widening of tropical overturning: Forced change, natural variability, and recent trends. *Journal of Geophysical Research: Atmospheres*, *124*(12), 6104-6119.

Taschetto, A. S., Ummenhofer, C. C., Stuecker, M. F., Dommenget, D., Ashok, K., Rodrigues, R. R., & Yeh, S. W. (2020). ENSO atmospheric teleconnections. *El Niño southern oscillation in a changing climate*, 309-335.

Trascasa-Castro, P, Y. Ruprich-Robert, F. Castruccio, and A. C. Maycock, (2021). Warm Phase of AMV Damps ENSO Through Weakened Thermocline Feedback. *Geophysical Research Letters*, 48(23):e2021GL096149. ISSN 1944-8007. doi: 10.1029/2021GL096149.

Trenberth, K. E., Branstator, G. W., Karoly, D., Kumar, A., Lau, N. C., & Ropelewski, C. (1998). Progress during TOGA in understanding and modeling global teleconnections associated with tropical sea surface temperatures. *Journal of Geophysical Research: Oceans*, *103*(C7), 14291-14324.

Turco, M., Jerez, S., Doblas-Reyes, F. J., AghaKouchak, A., Llasat, M. C., & Provenzale, A. (2018). Skilful forecasting of global fire activity using seasonal climate predictions. *Nature Communications*, 9(1), 1-9.

Wallace, J. M., & Hobbs, P. V. (1977). Atmosphere science - An introductory survey. *Atmosphere science-an introductory survey*, V.

Walker, G. T., & Bliss, E. W. (1932). Memoirs of the royal meteorological society. World weather V, 4, 53-84.

Wang, G., & Cai, W. (2020). Two-year consecutive concurrences of positive Indian Ocean Dipole and Central Pacific El Niño preconditioned the 2019/2020 Australian "black summer" bushfires. *Geoscience Letters*, *7*(1), 1-9.

Wang, Y., & Huang, P. (2022). Potential fire risks in South America under anthropogenic forcing hidden by the Atlantic Multidecadal Oscillation. *Nature Communications*, *13*(1), 2437.

Zhang, T., Shao, X., & Li, S. (2017). Impacts of atmospheric processes on ENSO asymmetry: A comparison between CESM1 and CCSM4. *Journal of Climate*, *30*(23), 9743-9762.

Zaplotnik, Ž., Pikovnik, M., & Boljka, L. (2022). Recent Hadley circulation strengthening: a trend or multidecadal variability?. *Journal of Climate*, *35*(13), 4157-4176.

Acknowledgments

P.T.-C. was supported by a PhD scholarship from the Natural Environment Research Council PANORAMA Doctoral Training Partnership (NE/S007458/1). Y.R.-R. received the support of a fellowship from "la Caixa" Foundation (ID 100010434) and from the European Union's Horizon 2020 research and innovation programme under the Marie Skłodowska-Curie grant agreement No 847648. The fellowship code is LCF/BQ/PR21/11840016. A.C.M. was supported by the European Union's Horizon 2020 research and innovation program under grant agreement no. 820829 (CONSTRAIN project) and The Leverhulme Trust (PLP-2018-278). M.T. acknowledges funding by the Spanish Ministry of Science, Innovation and Universities through the Ramón y Cajal Grant Reference RYC2019-027115-I and through the project ONFIRE, grant PID2021-123193OB-I00, funded by MCIN/AEI/ 10.13039/501100011033. Computing facilities were provided by the Barcelona Supercomputing Center and the University of Leeds. We thank Gokhan Danabasoglu and

Fred Castruccio for providing the climate model output, and two anonymous reviewers for their constructive feedback, which helped to improve the readability and quality of this paper